Sliding Mode-Based Control of an Electric Vehicle Fast Charging Station in a DC Microgrid

Amjad Muneim Mohammed[1], Siham Naser Hendi Alalwan[1], Akın Taşcıkaraoğlu[1,*], and João P. S. Catalão[2]

[1]*Department of Electrical and Electronics Engineering, Mugla Sitki Kocman University, Mugla, Turkey*

[2]*Faculty of Engineering of the University of Porto and INESC TEC, Porto 4200-465, Portugal*

[*]*akintascikaraoglu@mu.edu.tr*

Abstract

The fast-charging units have become a more efficient and attractive option recently for reducing the challenges due to the long charging time of electric vehicles (EVs). To evaluate the impacts of the EV fast charging stations (EVFCS) on the power grid and also to assess their contributions to the system operation through the vehicle-to-grid (V2G) technology, two control methods, namely, sliding mode control (SMC) and fuzzy logic control (FLC), are developed in this study for a DC microgrid including EVFCS and distributed generation sources. In these methods, the EV battery is used as a DC source of a distribution static compensator (D-STATCOM) with the objective of mitigating the voltage sag in the microgrid. Various simulations are conducted in MATLAB Simulink/SimPowerSytems environment in order to examine the effectiveness of the proposed control approaches in terms of ensuring the stability and improving the dynamic performance of the EVFCS. The results show that considerable improvements can be achieved, especially in the case of using the SMC method.

Keywords: Electric vehicle fast charging stations; fuzzy logic control; microgrid; sliding mode control; V2G.

1. Introduction

The number of electric vehicles (EVs) on the road has been considerably increasing at the last years due especially to their increasing efficiency and range. The EV number worldwide is estimated to surpass 250 million in the next decade [1].

One of the primary factors hindering their growth is the long charging periods of EVs caused by the limited charging rate of EV charging units. The slowest charging unit, namely, Level 1 charging, uses a standard household outlet and a plug to connect to the onboard charger of EVs whereas Level 2 charging provides power at 230 V and up to a current

of 30 A via a specific equipment at home or at a charging station. Level 1 and level 2 chargers are generally convenient to use during night times or working periods since it takes four to sixteen hours to fully charge a depleted battery [2]. Thus, the level-3 DC EV fast charging units, which can charge an EV in about 30 minutes, were developed and started to be used commercially. Their high charging power ranging from 50 to 240 kW, however, poses an additional strain on the power grids [3]. Also, these units can cause the increase of greenhouse gas emissions indirectly as the majority of their energy requirement could be supplied by the conventional power plants. Besides, the nonlinear characteristics of the EV fast charging units lead to power losses and voltage fluctuations [4]. These problems are particularly crucial for the residential level-3 DC EV fast charging units since they are directly connected to the distribution network.

Using the EV fast charging stations (EVFCSs) in microgrid environments coupled with renewable energy-based distributed generation systems (DGSs) has been emerging as one of the most promising solutions to the abovementioned problems as the DGSs are decentralized and flexible technologies. A control method was proposed in [5] for maintaining the state-of-charge (SOC) of an energy storage system (ESS) and DC bus voltage within the predefined limits in a microgrid, including photovoltaic (PV) panels, EVFCSs, and an ESS. The economic benefits of integrating a PV system and EVFCSs and in a microgrid environment were assessed in [6]. Another PV-integrated DC microgrid was considered in [7] in which a control method was used for exploiting the PV power generation. The authors in [8] proposed a charging approach for EV charging stations (EVCSs) in microgrids for reducing the charging times by also taking the battery health into account. Considering the benefits of both system operator and consumer, the authors in [9] presented a DC microgrid with rooftop PV units and EVFCSs.

The studies mentioned above show that the charging power of the EVs can be provided with higher economic benefits and less power losses when the EVFCSs are located in a microgrid structure. Besides, the EVs connected to EVFCSs can support the distribution system operation while using the available energy in the EV batteries, which is called vehicle-to-grid (V2G) technology. A V2G-based energy management method was presented in [10] for EVCSs within a microgrid with the objective of balancing the generated power and total load demand.

A V2G scheduling strategy based on frequency control was put forward in [11] for protecting the EV batteries, especially during the grid connections. In order to optimize the EV charging and discharging profiles, the authors in [12] developed an energy management method based on generation and consumption forecasts for microgrids,

including PV units and an EV parking lot. The charging and discharging profiles were also considered in [13] to increase the number of EVs connected to a microgrid.

Even though the V2G technology has been used for providing energy to the distribution systems when needed in the literature reviewed above, none of these studies except for a previous study of the authors [14] examined the use of EV battery as a DC voltage source in a distribution static compensator (D-STATCOM) system in V2G mode. In this study, first, a DC microgrid including solar PV arrays and level-3 EVFCS, which is a modified version of the microgrid considered in [14] with different system components, is designed and a control strategy based on controlling the converters of the PV arrays and EVFCS adaptively is proposed with the objectives of alleviating the impacts of voltage sag and decreasing the EV charging times by also considering the V2G interactions. Furthermore, to reduce the overshoot in the voltage at the DC bus, intelligent control methods, namely sliding mode control (SMC) and Fuzzy logic control (FLC), are used for controlling the bidirectional converter of EV charger, due to several reasons such as: (i) the conventional controllers adopted in the literature, such as the proportional-integral (PI) controller used in [14], have overshooting problem with high settling times and limited robustness against uncertainties, resulted in low responses to fast changes, (ii) the design of these conventional controllers for nonlinear systems requires the mathematical model of the plant, making the design process more difficult and time-consuming [15, 16], (iii) advanced controllers such as predictive controller [17] and hierarchical controller necessitate advanced analytical skills, and (iv) intelligent methods are already used for different power system operations with reasonable performance to overcome these problems [5, 18, 19].

The main contributions of the presented study are given as follows.

1. A low-voltage DC microgrid including EVFCS with V2G technology and PV systems is introduced.
2. The batteries of EV connected to an EVFCS are used as a DC source of a D-STATCOM system.
3. Improved control strategies based on the SMC and FLC methods are developed to mitigate the overshoot in the EV battery voltage and peak of the initial current.

The remaining sections are organized as follows: the considered system structure is described in Section II and Section III explains the proposed control approach. Section IV elucidates the EV battery-integrated D-STATCOM and the simulation studies with comparisons are provided in Section V. Lastly, Section V draws the conclusions.

2. System Description

In this study, a grid-connected microgrid including EVFCS and a solar PV array with a peak power of 120 kW operating at the maximum power point tracking (MPPT) mode is considered as shown in Fig. 1. Due to its benefits in the improvement of power grid peak performance, a DC microgrid is considered and PV arrays are preferred as DGSs since the PV power generation provides higher flexibility for the integration with the EVFCSs compared to stochastic wind power generation. The considered system parameters are given in Table I.

As can be seen from Fig. 1, the EVFCS is connected to the DC bus through a bidirectional DC/DC charger for controlling the charging of the EV and the PV string is linked to the DC bus through a DC/DC converter. Besides, in order to ensure a high-power supply to the EVFCS in the case of simultaneous charging of the units, all the system components are connected to a 900 V low voltage DC bus (LVDC bus). The grid connection is realized through a bidirectional AC/DC inverter and a transformer. The control of the inverter is modulated through the pulse width modulation (PWM) signals generated by the outer voltage loop and inner current loop PI controller based on the model presented in [20]. The details of the main components of the system considered in this study are described in detail in the following subsections.

A. Design of PV system and its control algorithm

The PV array is composed of 1Soltech 1STH-215-P panels whose electrical specifications are presented in Table I. The PV model adopted for this system [5, 21, 22] is based on a controllable current source, a diode in parallel with the current source, a parallel and a series resistance, as depicted in Fig. 2. The equation used for the PV cell's current-voltage relationship, which provides a good trade-off between the accuracy and simplicity [21], is given by (1):

$$I = I_p - I_s\left(e^{q(V+IR_s)/(nKT)}\right) - \frac{(V+IR_s)}{R_{pa}} \tag{1}$$

where I_s is the diode saturation current and I_p is the PV current, which can be calculated by the following expressions:

$$I_p = I_{p0}\left(1 + k_1(T - 300)\right) \tag{2}$$

$$I_s = k_2 T^3 e^{(qV_G/KT)} \tag{3}$$

where I_{p0} is the PV current at $300°K$, V is the PV output voltage, K is Boltzmann constant; $k_1$and k_2 are the constants related to PV characteristics [23], n is diode quality factor, q is the electric charge of an electron, V_G is the voltage across diode terminals, and T is PV operating temperature.

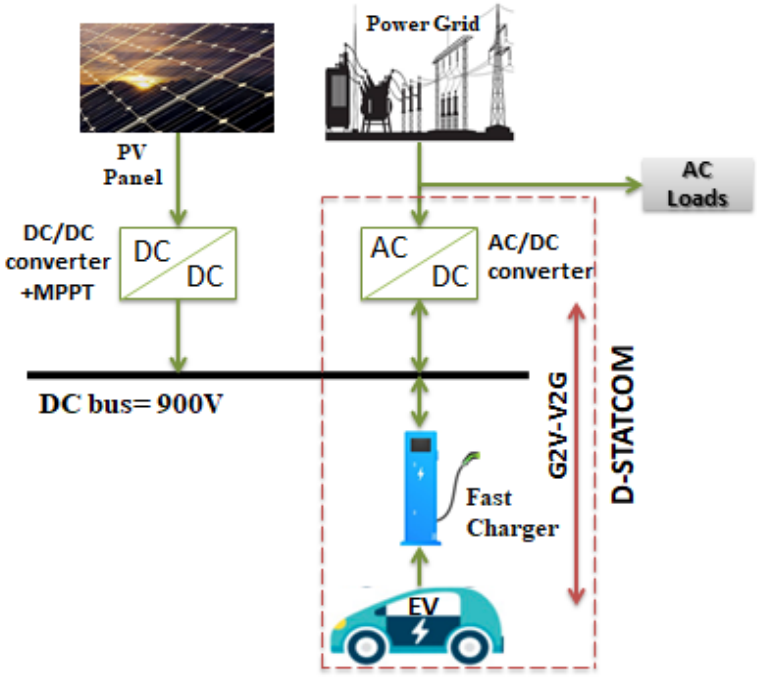

Fig. 1. *Proposed microgrid structure.*

Table I Main parameters of the DC microgrid and EVFCS

Parameter	Values
PV, Number of modules in series, NS	10
PV, Number of modules in parallel, NP	50
PV system converter, L	2×10^{-5} H
PV system converter, C_{PV}	1×10^{-3} F
PV system converter, C_{DC}	2600×10^{-6} F
Grid voltage, V_{grid}	25×10^{3} V
Filter, L_{grid}, L_{inv}	100×10^{-6} H
Filter, C_{filter}	50×10^{-6} F
EV Battery nominal voltage, V_b	480 V
EV Battery rated Capacity, C_b	100 Ah
EV battery Response time, T	10^{-3} Sec
EV bidirectional charger, L_{char}	10.85×10^{-6} H
EV bidirectional charger, C_{char}	100×10^{-6} F

A DC/DC boost converter is utilized to connect the PV array to the DC microgrid. In order to overcome the undesirable effects on the PV output power and draw the maximum power, the PV system operates in MPPT and voltage control mode [24]. The MPPT is achieved using a PI voltage controller and the incremental conductance MPPT method is applied to adjust the DC output voltage of the PV system. In this method, the array terminal voltage is regulated depending on the MPP voltage, which is based on the cumulative and instantaneous conductance of the

PV module. This algorithm provides a good yield method while the atmospheric conditions are rapidly changing. It also accomplishes lower oscillation around the MPP than the perturbation and observation (P&O) method.

B. Design of EVFCS

The equivalent circuit of the proposed EVFCS model is shown in Fig. 3 [20]. A lithium-ion EV battery, which is widely used due to its longer life-cycle, higher energy and power density compared to other battery types [25], is considered in the study. The battery model, which is a modified version of the model available in the SimPowerSystems, consists of one variable voltage source and one series resistance [23]. The SOC value is monitored so as to avoid deep battery discharge or an overcharge. The battery output voltage and SOC are calculated as follows [26]:

$$V_{Batt} = E_{Batt} - I_{Batt} \cdot R_0 \tag{4}$$

$$SOC(\%) = SOC_{int}(\%) - 100\left(\frac{\int I_{Batt} \cdot dt}{q}\right) \tag{5}$$

where q represents the maximum capacity of the battery, E_{Batt} is the open circuit battery voltage depending on the battery operating mode, I_{Batt} is the EV battery current and R_0 is the internal resistance.

The EV battery is connected to the DC bus through the off-board charger for fast charging. A bidirectional DC/DC converter with two IGBTs operated by complimentary control signals forms the basic element of the off-board charger. The EV charger enables a bidirectional power flow to utilize PV and grid power for EV charging while also supplying power to distribution system in the case of excess power [27, 28].

During the charging mode, the upper switch ($Sw1$) operates with the required duty cycle, and the converter steps down the input voltage (V_{dc}) to battery charging voltage (Vb) acting as a buck converter. During this period, the current flows to the battery through the switch and inductor where the power flow is from the grid and PV to vehicle. In the discharging mode, the lower switch ($Sw2$) operates, the converter steps up Vb to V_{dc} acting as a boost converter and the current continues to flow over the inductor and completes its circuit through the $Sw1$ diode and capacitor. The power flow is from EV battery to grid in this case [29]. With d being the $Sw1$ duty ratio and d' being the $Sw2$ duty cycle, the battery voltage during buck mode and the output voltage during boost operation mode are calculated by [20]:

$$Vb = V_{dc} \times d \tag{6}$$

$$V_{dc} = \frac{Vb}{1 - d'} \tag{7}$$

C. Design of grid-connected inverter

A bidirectional AC/DC voltage source inverter (VSI) connects the DC microgrid to the grid through a step-down transformer and a LCL filter shown in Fig. 4. The bidirectional VSI converts the DC bus voltage into AC voltage [24]. The three-phase transformer steps down the voltage from the grid voltage level to EVCS voltage level and the grid-connected inverter converts the AC power into DC power, forming a DC bus. The passive LCL filter with the parameters given in Table I is attached at the inverter outputs for obtaining a pure sinusoidal current and voltage. The parameters of the LCL filter, namely, inverter side inductance L_{inv}, filter capacitance C_{filter}, and source side inductance L_S are defined and calculated using the method given in [27, 30, 31]. Besides, the inverter side inductance is chosen based on the DC voltage, switching frequency, current total harmonic distortion and inverter modulation index. The grid source parameters, resonance frequency, reactive power and ripple attenuation factor all determine the selection of source side inductance and capacitance.

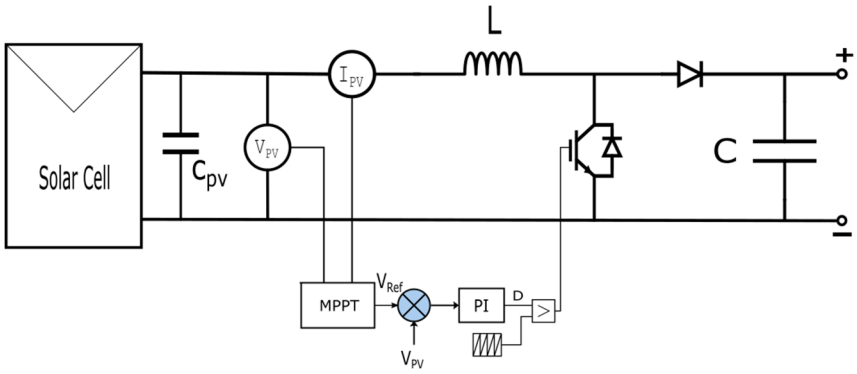

Fig. 2. *PV array and MPPT control of DC/DC boost converter.*

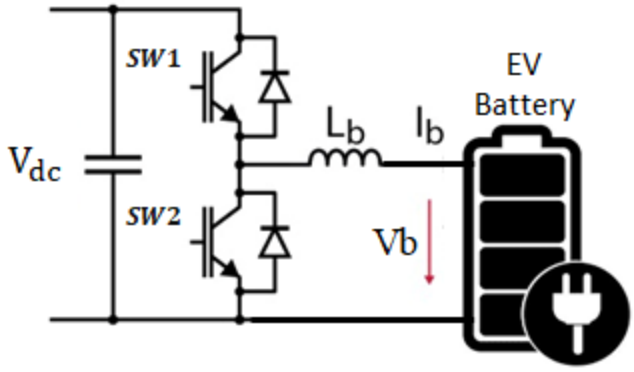

Fig. 3. Equivalent circuit model of EV battery and off-board charger [20].

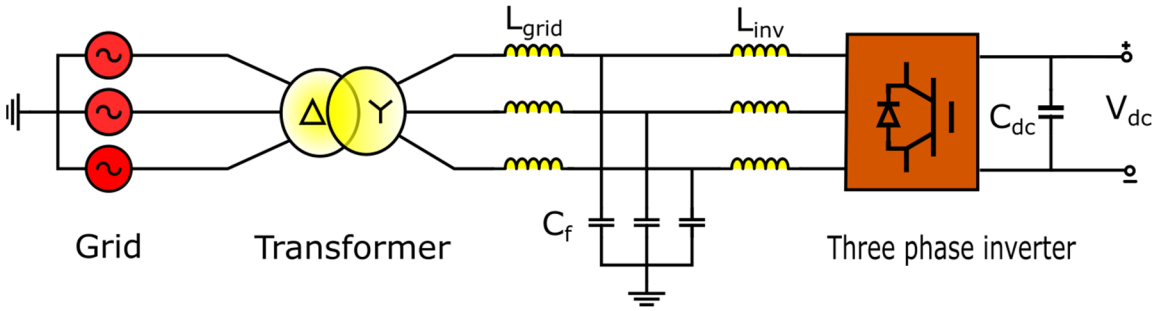

Fig. 4. *Three-phase inverter and LCL filter [20].*

3. Proposed Decentralized Control System

Control systems for the DC microgrids including EVFCSs can be centralized or decentralized. The advantages of the centralized control strategy include strong controllability and observability of the whole system; however, the centralized control has also several drawbacks such as reduced reliability, scalability and flexibility [5, 23]. Therefore, it is generally not practical for the energy management between generation units and EV demand, especially for the large power systems where the information to be collected is not limited. Unlike the centralized control, a decentralized control system (DCS) in which each EVFCS works independently from the rest of the system is adopted in this study since it enables the insertion of new components into EVFCS without disrupting the other system components. Independent controllers based on PI, SMC and FLC methods are developed for the power converters of the EV charger, PV panel, and utility grid. The ultimate focus of the independent controllers is to maintain the power balance in the EVFCS while controlling the LVDC bus at the voltage reference.

As for the PV system, the PV is assumed to work in MPPT and PI control mode to regulate the output DC voltage, as stated in Section II.A, since the main goal of the boost converter is to realize the MPPT by regulating the PV voltage

making use of the power voltage characteristic curve. The resulting signal from the MPPT is regulated using a voltage loop controller as the outer voltage of the MPPT is compared with the PV panel voltage and the duty cycle of the boost converter is determined by the PI controller. The output voltage of the PV system is hence prevented from exceeding the adjusted value.

A. Inverter control

The main target of the AC/DC VSI inverter is to keep the DC bus voltage at 900V for EVFCS. The DC bus voltage is adjusted to a constant value while energy generation or load demand varies in order to maintain the power exchange between the EVFCS and grid. In this study, a dq control method comprised of one outer voltage loop and two current loops is applied using three PI controllers. Besides, a phase locked loop (PLL) is performed to synchronize with the grid voltage [32].

The proposed inverter control system is depicted in Fig. 5, in which the d-axis outer loop adjusts the DC bus voltage and the inner loop adjusts the active AC current. The PLL receives the AC source voltage as input and the output V_d, and frequency signals are determined in the dq frame inverter control [33]. The reactive current I_q is set to zero. The PI controller gains, namely, the proportional gain, K_p and integral gain K_i are selected as 4.5 and 200, respectively.

B. EV charger control

Since the nonlinear elements in bidirectional DC/DC converters cause dynamic nonlinear equations, improved control strategies based on FLC and SMC are proposed to enhance the system design. The main objective of the proposed controllers is to reduce the voltage overshoot and initial peak current of the EV battery, and keep the fast-charging current constant. The control system also includes a PWM generator to provide pulses to the DC/DC charger's IGBTs.

Two identical control mechanisms can be developed depending on the desired charge method: constant current (CC) and constant voltage (CV). The CV strategy is equivalent to using the battery as a voltage source, and the controller output determines the buck-mode operation of the EV charger while the CC control is equivalent to using the battery as a current source, and the output determines the boost-mode operation [30, 34]. A CC control mechanism is employed in this study and the bidirectional charger is set by changing the value of the duty cycle (d). When the

battery current is not equal to the reference current, the control system activates. If the current exceeds the reference current, the value of d is reduced. If the battery current is less than the reference current, the d value is enlarged.

1) Fuzzy Logic Control

A FLC-based controller is used in this study due to the lack of reliance on historical data and its easy adaptability to complex systems, which is generally required by the other similar controllers.

Figure 6 depicts the functional block diagram of the FLC. The FLC is used in the proposed EVFCS for obtaining constant charging/discharging current at various conditions. It consists of three stages, namely, the fuzzification stage, the processing stage (fuzzy rule algorithm), and the de-fuzzification stage [35]. The input of the FLC model is the reference battery current error, which is calculated as the difference between the EV battery current and actual battery current while the output parameter of the fuzzy controller is the duty cycle.

The membership functions of the FLC used are shown in Fig. 7. Figure 7 (a) represents the membership function (MF) inputs while Fig. 7 (b) represents the output MF. Five MFs with values varying between -1 and 1 are selected for the error (E), change of the error (∇E) and control output (∇d), which are Negative Big (NB), Negative small (NS), Zero (Z), Positive small (PS), and Positive Big (PB). The manipulation efforts required to obtain the control output might be reduced considerably with a very small steady-state error thanks to these membership functions [5]. Table II shows the 25-rule foundation used for FLC as various changes to the PWM control signal are needed to bring the charging current back to its desired value.

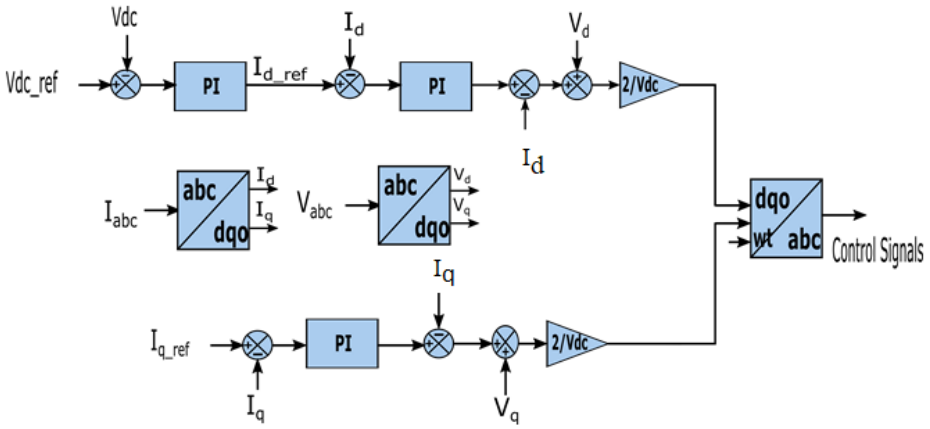

Fig. 5. *Inverter control system.*

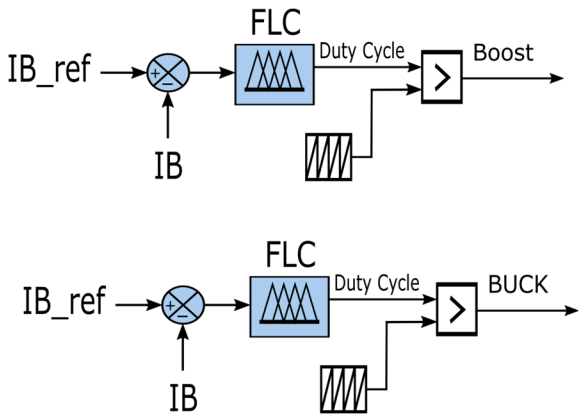

Fig. 6. *Fuzzy logic control scheme for bidirectional charger.*

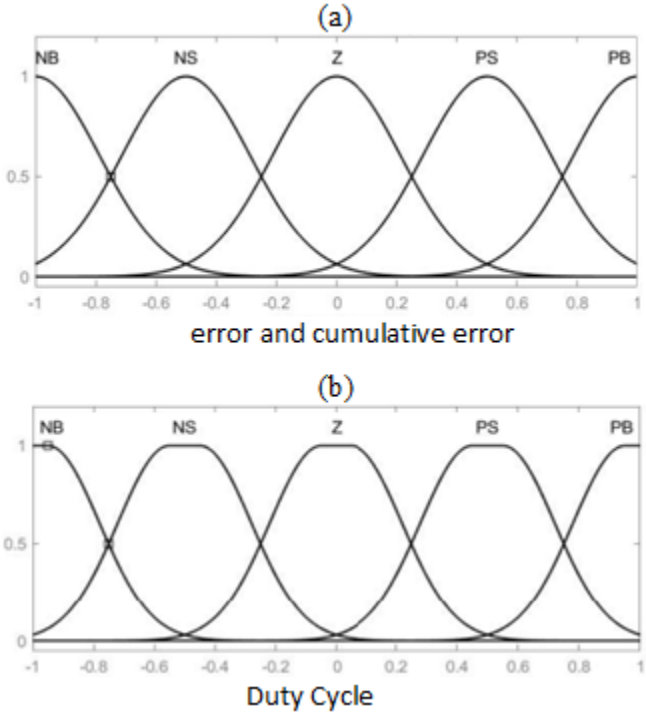

Fig. 7. *Membership functions for the considered FLC: (a) inputs (error and cumulative error), (b) output.*

Table II Rule base for EV charger control

∇E \ E	NB	NS	Z	PS	PB
NB	NB	NB	NB	NS	Z
NS	NB	NB	NS	Z	PS
Z	NB	NS	Z	PS	PB
PS	NS	Z	PS	PB	PB
PB	Z	PS	PB	PB	PB

2) Sliding Mode Control

SMC is a nonlinear controller that handles the transient oscillation and slow response caused by dynamic load changes. This method is especially effective for variations and disturbances with low sensitivity [19]. The SMC generally involves the current control loop and its nonlinear dynamic nature make it an ideal option for battery charging applications [36, 37].

Figure 8 shows the SMC model considered in the study. The proposed SMC current controller employs the output current error as the controlled state variable, which allows the battery current to follow the desired reference current closely. To have a fast response in bidirectional converters, the battery current reference should be always tracked.

The sliding surface S of the proposed controller is selected as a combination of two state variables with a switching function $u = 0.5(1 + \text{sign}(S))$ in which u represents the logic state of the switch. The switching function can be expressed as [37]:

$$S = \alpha_1 x_1 + \alpha_2 x_2 \tag{8}$$

where α_1 and α_2 represent the sliding coefficients, which are selected based on trial-and-error method. These coefficients also represent the band of switching oscillation that is related to the boundary of the system uncertainty. The current error, x_1 and the integral of the current error, x_2, are the controlled state variables, which are given as:

$$x_1 = i_{ref-i_{bat}} \tag{9}$$

$$x_2 = \int x_1 \, dt = \int \left(i_{ref-i_{bat}}\right) dt \tag{10}$$

where i_{bat} denotes the instantaneous battery current. Ideally, only the controlled variable x_1 is required in the SMC current controller at an infinitely-high switching frequency to ensure that the output current is controlled to exactly follow its reference, i.e., $i_{bat} = i_{ref}$.

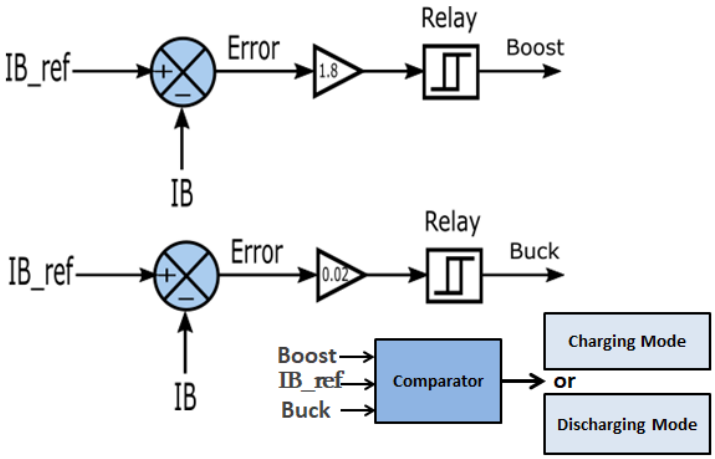

Fig. 8. *Sliding mode control for bidirectional EV charger.*

4. Voltage Improvement with EV Battery-Integrated D-STATCOM

An EV battery with V2G technology can contribute to grid stability [38] and be used for different power system applications such as valley falling or peak shaving. As stated before, to improve power quality, it can be also utilized as a DC voltage source in a D-STATCOM.

D-STATCOM is a shunt device that is typically connected near the load at power grids to compensate the harmonics, voltage sag and voltage swell [39]. D-STATCOM consists of a VSI, an LC filter, a DC source and a control circuit, as shown in Fig. 9 [14]. The design procedure of the D-STATCOM during V2G mode for this study is adapted from [40].

In this study, an EV battery with a SMC-based controller is employed as a DC source in the D-STATCOM. An FLC-based control approach depicted in Fig. 10 is developed for D-STATCOM to control the required voltage at the point of common coupling (PCC). Table III shows the 49-rule foundation and Fig. 11 represents the input and the output MFs used for FLC of D-STATCOM. The EV battery is discharged with the CC-CV during the V2G mode. In this mode, the bidirectional converter and D-STATCOM DC-side voltages are maintained at a predefined value of 700 V and the battery delivers the constant current and voltage to the grid, resulted in a decrease in the SOC level. The parameters for the proposed system are presented in Table IV [14].

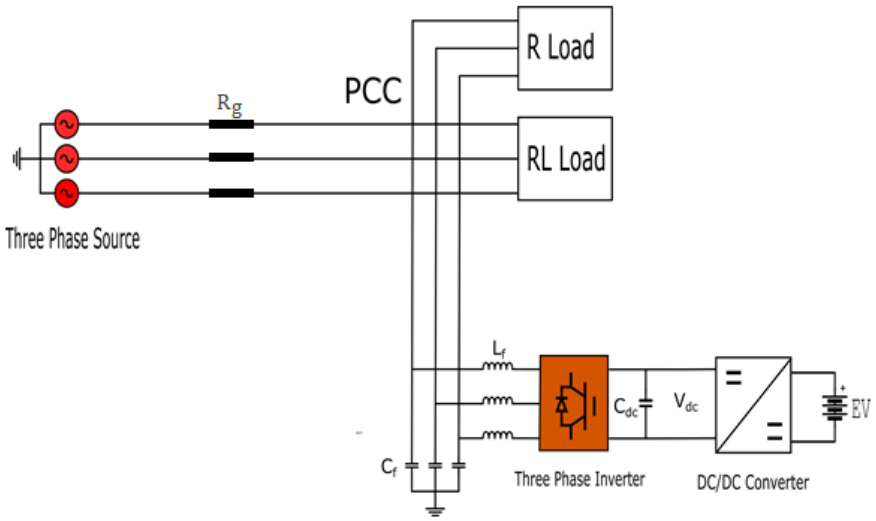

Fig. 9. *Block diagram of D-STATCOM device* [14].

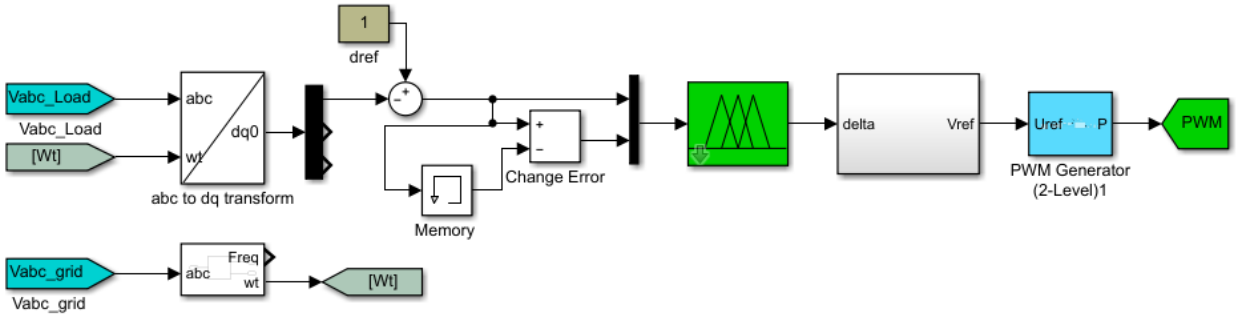

Fig. 10. *FLC scheme for D-STATCOM.*

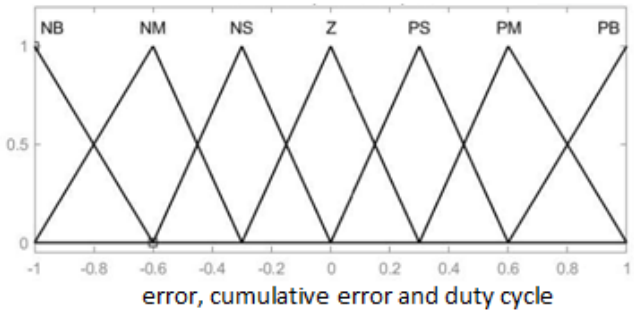

Fig. 11. *Membership functions for inputs and output variables of FLC.*

Table III Rule base for D-STATCOM control

E / ∇E	NB	NM	NS	Z	PS	PM	PB
NB	NB	NB	NB	NM	NM	NS	Z
NM	NB	NB	NM	NM	NS	Z	PS
NS	NB	NM	NM	NS	Z	PS	PM
Z	NM	NM	NS	Z	PS	PM	PM
PS	NM	NS	Z	PS	PM	PM	PB
PM	NS	Z	PS	PM	PM	PB	PB
PB	Z	PS	PM	PM	PB	PB	PB

Table IV D-STATCOM parameters [14]

Blocks	Parameter	Value
Three-phase voltage sources	Vrms (ph − ph)	400 V
	Frequency, f	50 Hz
R Load	Vrms (ph − ph)	400 V
	Power, P	20 kW
RL Load	Vrms (ph − ph)	400 V
	Power, P	20 kW
	Reactive power, Q	100 Var

5. Simulation Results

Various simulations for EVFCS with onboard charging, discharging, and D-STATCOM modes are conducted in MATLAB Simulink/SimPowerSystems to validate the proposed DCS for distributed integration of PV and EVFCS in a grid-connected DC microgrid. Different operating scenarios and control methods are simulated to validate the performance of the system in controlling the supplying power to the EVFCS and DC voltage. Furthermore, the benefits of making use of a D-STATCOM device in V2G mode with SMC and FLC methods are provided to maintain the PCC voltage at its nominal value when a sag occurs in the distribution system voltage.

A. Considering only the EV battery charging

As stated above, a DC microgrid including a PV panel and EVFCS is considered in this study. The solar irradiance profile and the extreme power obtained from the PV array by MPPT for the corresponding solar irradiation are shown in Fig. 12. The total energy generated by the PV system is delivered to the EVFCS. The power curve in Fig. 12 (a) matches exactly the solar irradiance variation shown in Fig. 12 (b). It can be observed that the irradiance is quite high for the first 0.4 s (1000 w/m^2, the standard condition) and the PV system delivers a power of 120 kW accordingly. Afterwards, the irradiance and the corresponding power generation values gradually decrease and reach 200 w/m^2 and 20 kW at the end of the considered simulation period.

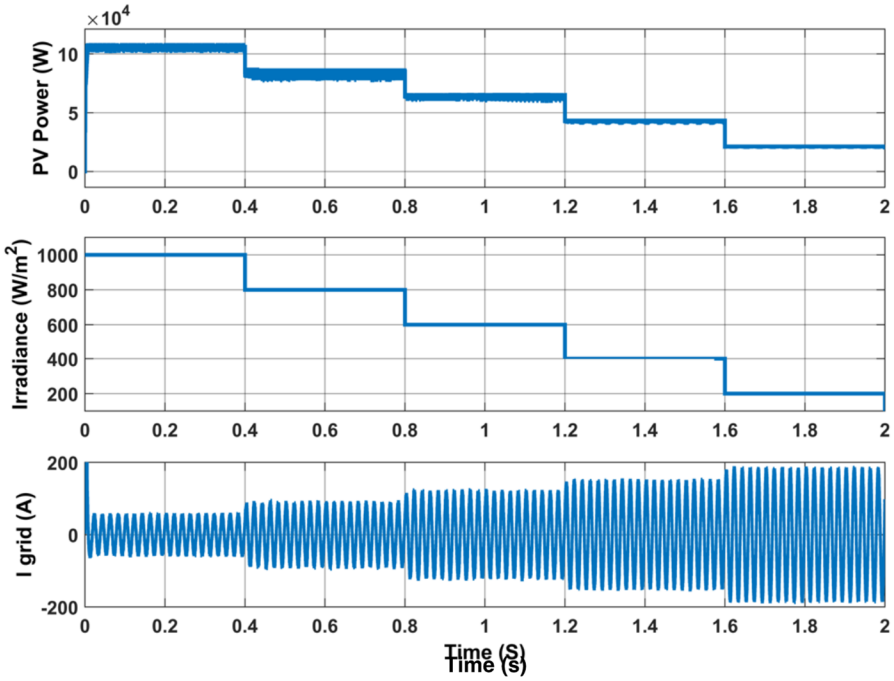

Fig. 12. *Change in: (a) power generated by the PV system, (b) sun irradiance, (c) AC current of utility grid.*

When the PV system is unable to meet the required EV battery and DC load power demand, the grid energy is used. As can be seen from Fig. 12 (c), the grid compensates the gap in power between the FCS, DC load demand and the PV supply by providing a current between 50 A and 190 A. The continued power supply to the EVFCS and a constant power at the DC load under different solar irradiation levels are achieved as shown in Fig 13. The PI controller, which regulates the grid inverter based on IGBTs, maintains the DC bus voltage at 900V while minimizing overshoot and oscillations with a high level of efficiency under different charging conditions as shown in Fig. 14.

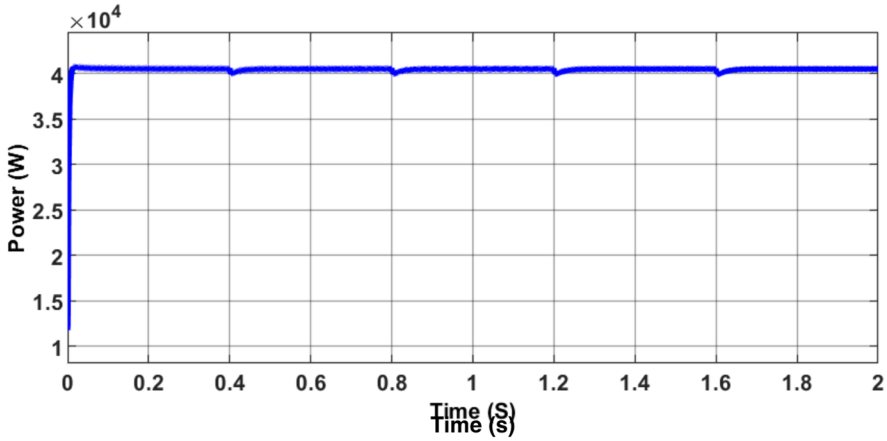

Fig. 13. *DC load power.*

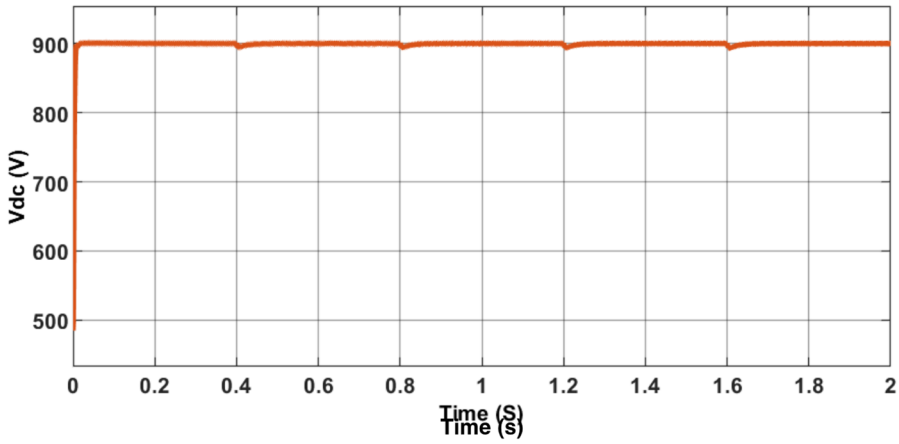

Fig. 14. *DC bus voltage for DC microgrid-to-vehicle mode.*

In this study, the bidirectional charger is designed for 534 V (output) with an input voltage of 900 V during DC microgrid-to-vehicle mode (charging mode). The voltage and capacity of the battery are selected as 480V and 100 Ah, respectively.

The simulation studies are conducted to test the proposed control approaches in the control of the charging current and voltage, and in the transition between different modes of operation. It is also noted that, a basic PI controller, which has been developed in a previous study of the authors [14], is used as a reference for the comparisons in order to validate the SMC- and FLC-based controllers.

1) The EVFCS with FLC

As stated before, the CC control mode is used for this configuration. The FLC controller generates the pulse to control the switch if the output voltage level exceeds or drops below a predetermined value. Figure 15 represents the voltage, current and SOC of the EV battery. The output voltage increases gradually and has less oscillations as shown in Fig. 15 (a). Similarly, the SOC increase gradually as shown in Figs. 15 (b). The peak of the initial current and overshoot are eliminated compared to the PI-controller [14], which can be seen from Fig. 15 (c) and the settling time obtained is 0.05 sec.

2) The EVFCS with SMC

Similar to the FLC-based controller, the CC control mode is used in this method. The SMC is proposed to regulate the error of EV battery current. The EV battery variables of the nonlinear SMC controller are presented in Fig. 16. As shown in Fig. 16 (a) and Fig. 16 (b), the overshoot, oscillations and initial peak current are completely eliminated. Figure 16 (c) refers to the battery SOC in this case.

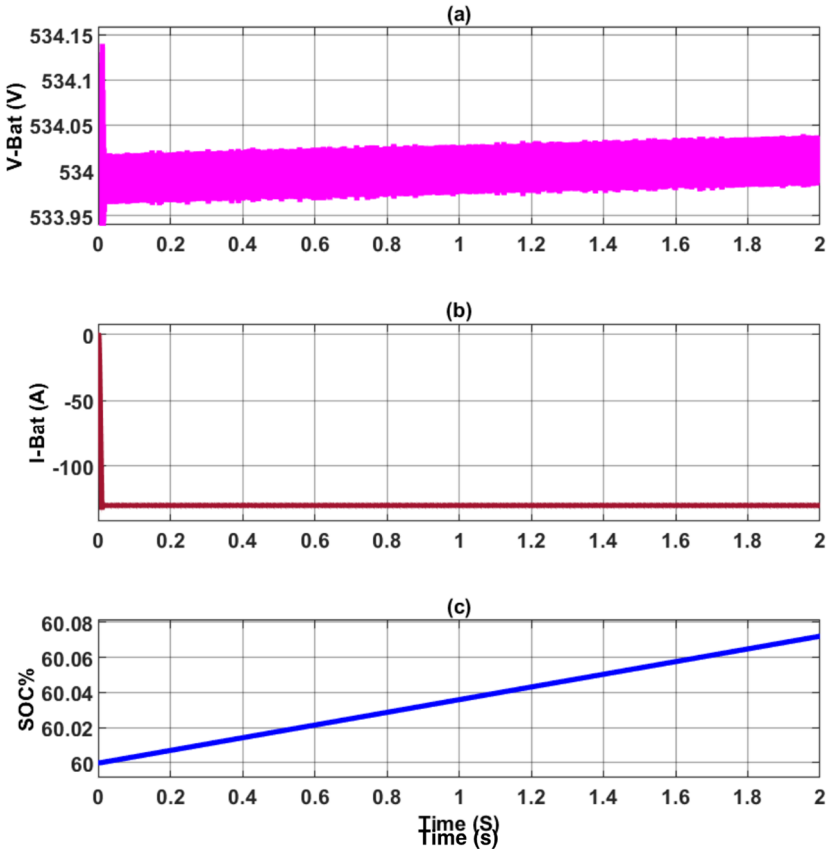

Fig. 15. *Variations during EV charging with FLC: (a) battery voltage (b) battery current, (c) battery SOC.*

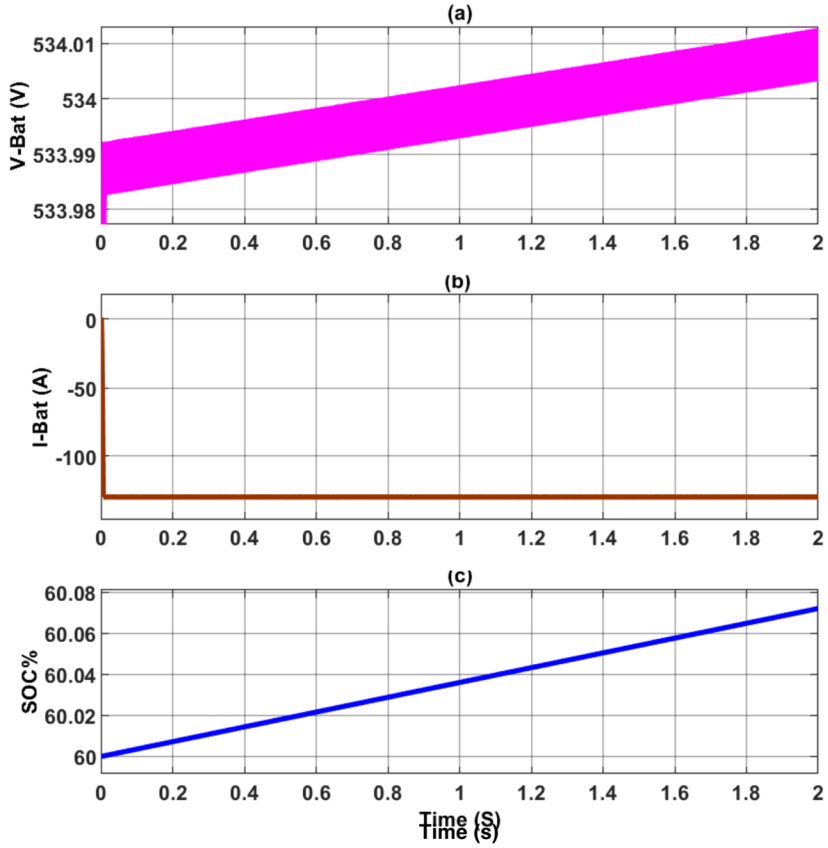

Fig. 16. *Variations during EV charging with SMC: (a) battery voltage (b) battery current, (c) battery SOC.*

A comparative analysis of SMC and FLC is made and the results are tabulated in Table V. The output current from SMC and FLC is equal to the reference current; however, the battery voltage ripples of SMC are very low compared to FLC controllers. It has a low settling time of around 0.02 seconds. Peak overshoot is completely eliminated in both the SMC and FLC controllers. As can be seen from the results, in the case of a nonlinear control system, SMC performs smoother operations due to the low settling time and fast response.

B. Considering G2V-V2G interactions

The EVFCS with off-board G2V-V2G integration is simulated in this section. Figure 17 shows the battery characteristics of the EV during charging (G2V) and discharging (V2G) processes. In G2V mode, the power flows from the grid to the EVFCS with a charging voltage of 534 V and an initial SOC of 60% from $t = 0$ to 1 sec, as shown in Fig. 17 (a) and Fig. 17 (c).

As shown in Fig. 17 (b), the CC control technique is used to achieve a constant fast charging and discharging current of 130 A as the maximum charging current of the Level 3 FCS has to be up to 80 A [41]. The VSC is responsible for DC-link voltage stabilization and providing the PCC voltage support control.

From $t = 1$ to 2 sec, the EV works in V2G mode. The power flows from the EV battery to the grid depending on the discharging power of the EV. The DC bus voltage starts to increase as shown in Fig. 18; however, the bidirectional charger based on the SMC controller and the inner current control loop of the inverter control tracking changes d-axis reference current, and quickly restores the DC-link at the desired voltage of 900 V by drawing more power from the EV battery to the grid as shown in Fig. 19.

The waveforms for voltage and current drawn from the grid by the EVFCS are shown in Fig. 20. It can be seen that a sinusoidal input current with less distortion is drawn by the EVFCS and the voltage is maintained at its nominal value during the G2V-V2G modes. There is no phase lag between the source voltage and source current as seen from Fig. 20, which shows that a high-power factor close to unity is obtained. During G2V operation, the voltage and current are in phase, and the power flow is 180° out of phase during V2G operation.

Table V Comparison of the performance of FLC and SMC

Parameter	**FLC**	**SMC**
Output voltage [V]	534	539.99
Peak overshoot [%]	0.026	0
Settling time [s]	0.05	0.02

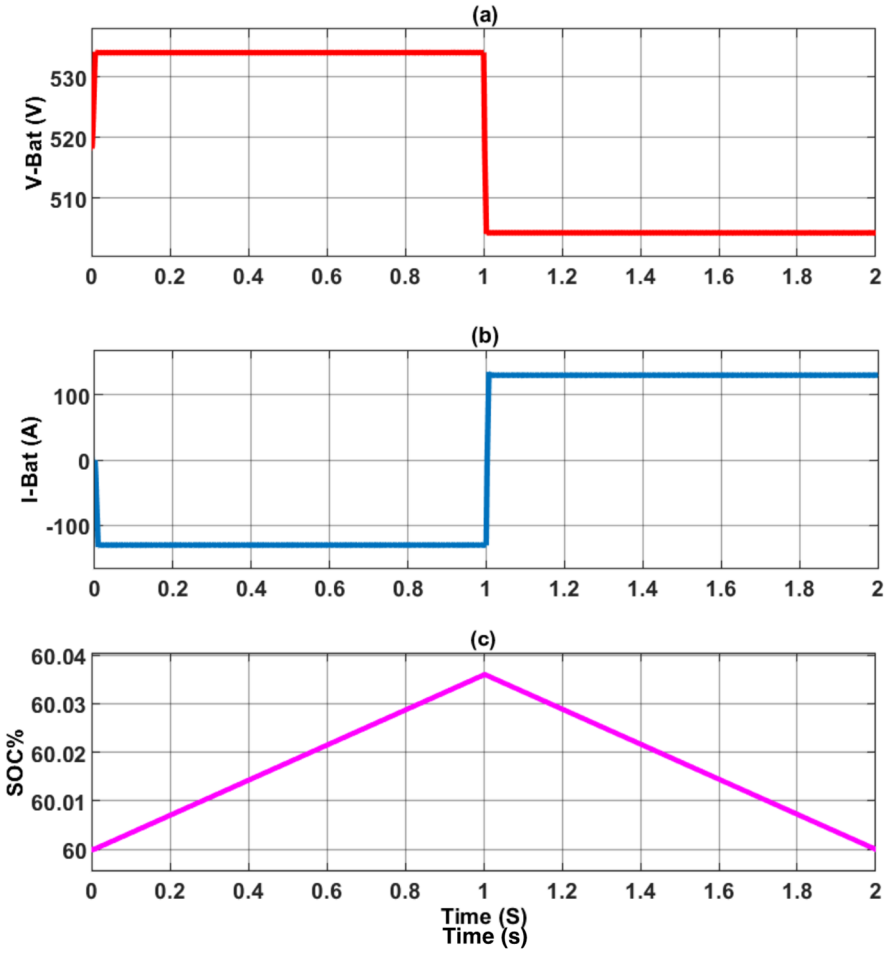

Fig. 17. *Variations during G2V-V2G operation: (a) battery voltage, (b) battery current, (c) battery SOC.*

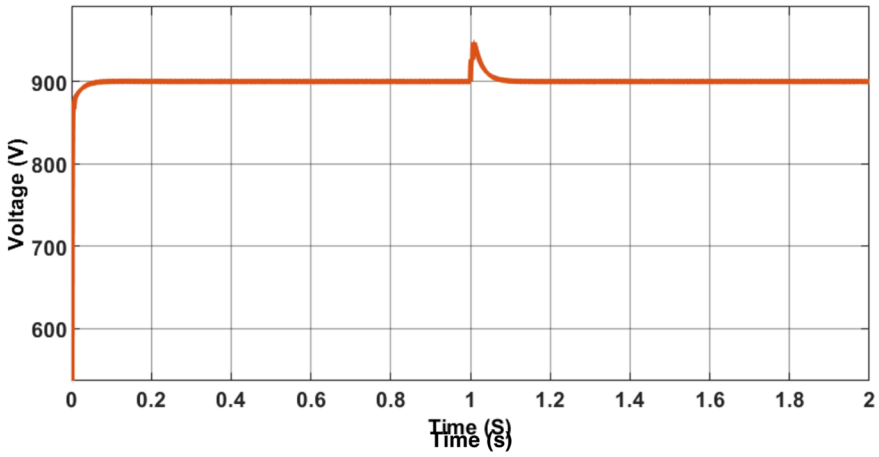

Fig. 18. *DC bus voltage for G2V-V2G operation.*

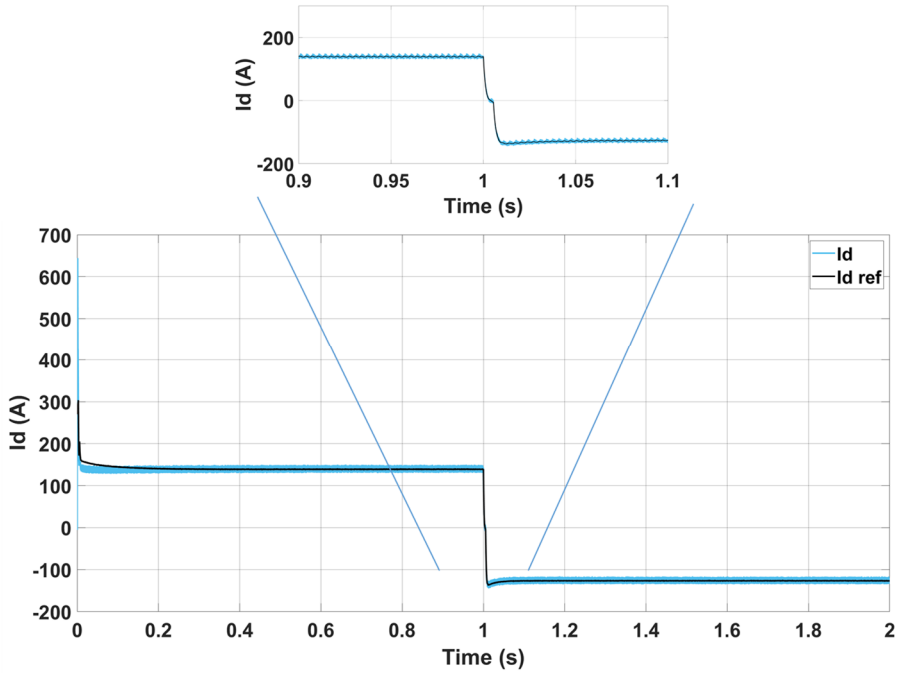

Fig. 19. *Id reference current tracking by inverter controller.*

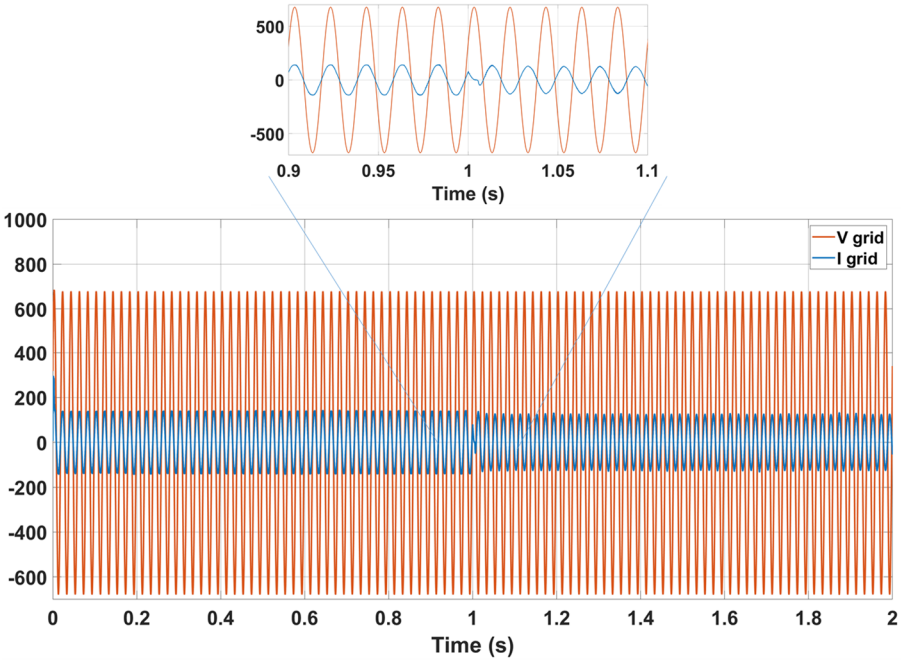

Fig. 20. *Grid voltage and injected current during V2G-G2V operation.*

C. Voltage sag mitigation with the EV battery-integrated D-STATCOM

Lastly, the EV battery is used as a power source in the D-STATCOM and the performance of SMC and FLC during discharging mode is investigated in the mitigation of the voltage sag.

As shown in Fig. 21, the voltage sag appears from 0.1 to 0.2 sec when a heavy load of 20 kW is included by switching $SW1$. The voltage drops by almost 30% of the normal voltage in this case, from 1 p.u. to 0.7 p.u. At 0.2 sec, the $SW1$ is opened and stays open until the end of the simulation time. The percentage of the sag is given by (11):

$$sag(\%) = \frac{V(p.u.) - V_{sag}(p.u)}{V(p.u)} \times 100 \tag{11}$$

As shown in Fig. 22, it is obvious that the voltage sag is reduced when the EV battery-connected D-STATCOM with FLC is integrated in the grid. The EV acts as a DC source during these periods and begins to release its stored energy. Figure 23 depicts the D-STATCOM DC-side voltage for V2G operation when the SMC controller is used. From the simulation results, it is seen that the SMC controller responds fast enough to track the sudden load change. They also prove that the FLC controller can generate the demand current for about 0.3 p.u. to support the voltage at the PCC for returning to rated voltage.

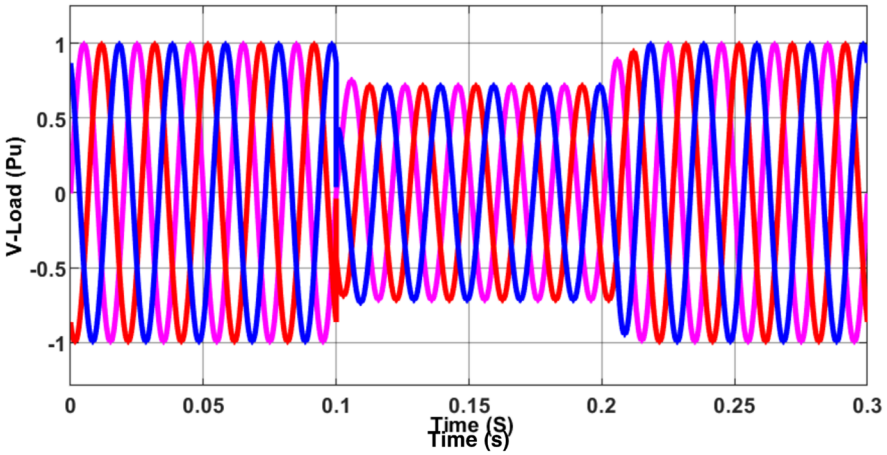

Fig. 21. *Three phase voltage at load point.*

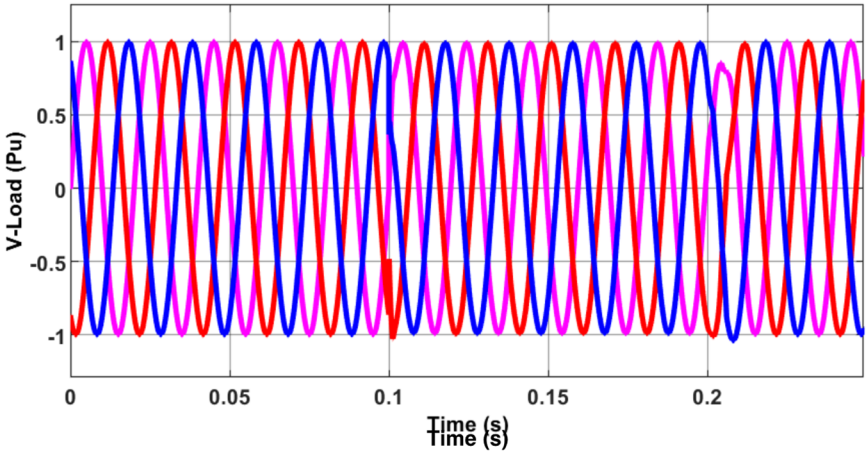

Fig. 22. *Three phase voltage at load point with D-STATCOM.*

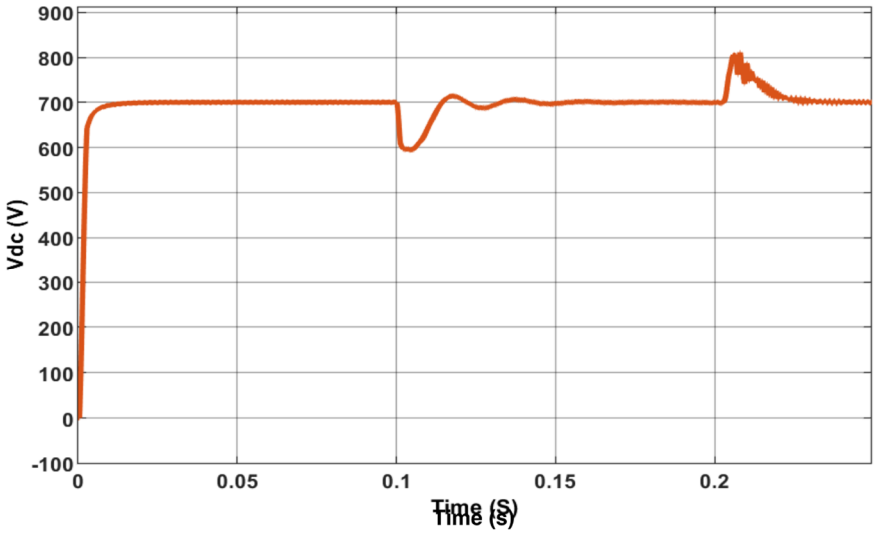

Fig. 23. *DC bus voltage for EV battery-connected D-STATCOM.*

6. Conclusion

In this paper, the modeling and design of a EVFCS in a microgrid with a DCS are presented to reduce the grid reliance and improve the power quality. A DC EVFCS with off-board chargers is developed to interface EVs to the microgrid-connected grid. The performance of the system is evaluated with two different control strategies: FLC and SMC controllers for EV fast chargers. The controllers use constant CC mode that regulates the output current of the EV charger. A comparison between these control types is conducted for the bidirectional fast charger. Besides, the utilization of an EV battery as a DC source of a D-STATCOM is considered to improve voltage profile. The D-STATCOM is built by integrating the FLC system, and implemented in MATLAB/Simulink/SimPowerSystems. The results of the case studies performed validate that the proposed FLC and SMC have less ripple, faster settling time and less peak overshoot. Also, the best performance is obtained in the case of using the SMC. The results also confirm that the proposed strategy can be effectively used to deal with the power quality problems by integrating the FLC-based DSTATCOM at the PCC to reduce voltage sag problem. The applicability and performance of the proposed approach will be validated on a power system with a higher number of components in a future study.

Acknowledgment

This work of A. Taşcıkaraoğlu is supported by Turkish Academy of Sciences (TUBA) within the framework of the Distinguished Young Scientist Award Program (GEBIP). Also, J.P.S. Catalão acknowledges the support by FEDER funds through COMPETE 2020 and by Portuguese funds through FCT, under POCI-01-0145-FEDER-029803 (02/SAICT/2017).

References

[1] International Energy Agency, "Global EV Outlook 2019: Scaling up the transition to electric mobility", 2019.

[2] M. Nour, H. Ramadan, A. Ali, and C. Farkas, “Impacts of plug-in electric vehicles charging on low voltage distribution network,” in *2018 International Conference on Innovative Trends in Computer Engineering (ITCE)*, 2018, pp. 357–362.

[3] X. Gong and J. Rangaraju, “Taking charge of electric vehicles-both in the vehicle and on the grid,” *Texas Instruments, Dallas, TX, USA*, pp. 1–13, 2018.

[4] A. K. Karmaker, S. Roy, and M. R. Ahmed, “Analysis of the impact of electric vehicle charging station on power quality issues,” in *2019 International Conference on Electrical, Computer and Communication Engineering (ECCE)*, 2019, pp. 1–6.

[5] P. García-Triviño, J. P. Torreglosa, L. M. Fernández-Ramírez, and F. Jurado, “Decentralized fuzzy logic control of microgrid for electric vehicle charging station,” *IEEE J. Emerg. Sel. Top. Power Electron.*, vol. 6, no. 2, pp. 726–737, 2018.

[6] L. Yang and H. Ribberink, “Investigation of the potential to improve DC fast charging station economics by integrating photovoltaic power generation and/or local battery energy storage system,” *Energy*, vol. 167, pp. 246–259, 2019.

[7] S. Wang, L. Lu, X. Han, M. Ouyang, and X. Feng, “Virtual-battery based droop control and energy storage system size optimization of a DC microgrid for electric vehicle fast charging station,” *Appl. Energy*, vol. 259, p. 114146, 2020.

[8] S. Wang, K. Kuang, X. Han, Z. Chu, L. Lu, and M. Ouyang, “A model-based continuous differentiable current charging approach for electric vehicles in direct current microgrids,” *J. Power Sources*, vol. 482, p. 229019, 2021.

[9] M. Dicorato, G. Forte, M. Trovato, C. B. Muñoz, and G. Coppola, “An integrated DC microgrid solution for electric vehicle fleet management,” *IEEE Trans. Ind. Appl.*, vol. 55, no. 6, pp. 7347–7355, 2019.

[10] F. Ahmad, M. S. Alam, S. M. Shariff, and M. Krishnamurthy, “A cost-efficient approach to EV charging station integrated community microgrid: A case study of Indian power market,” *IEEE Trans. Transp. Electrif.*, vol. 5, no. 1, pp. 200–214, 2019.

[11] Q. Yang *et al.*, “An improved vehicle to the grid method with battery longevity management in a microgrid application,” *Energy*, vol. 198, p. 117374, 2020.

[12] G. A. Salvatti, E. G. Carati, R. Cardoso, J. P. da Costa, and C. M. de O. Stein, “Electric vehiclesenergy management with V2G/G2V multifactor optimization of smart grids,” *Energies*, vol. 13, no. 5, p. 1191, 2020.

[13] O. Egbue and C. Uko, “Multi-agent approach to modeling and simulation of microgrid operation with vehicle-to-grid system,” *Electr. J.*, vol. 33, no. 3, p. 106714, 2020.

[14] S. N. H. Alalwan, A. M. Mohammed, A. Taşcıkaraoğlu, and J. P. S. Catalão, “An Improved Energy Management Strategy for a DC Microgrid including Electric Vehicle Fast Charging Stations,” in *2021 International Conference on Smart Energy Systems and Technologies (SEST)*, 2021, pp. 1–6.

[15] N. Hou and Y. Li, “The comprehensive circuit-parameter estimating strategies for output-parallel dual-active-bridge DC–DC converters with tunable power sharing control,” *IEEE Trans. Ind. Electron.*, vol. 67, no. 9, pp. 7583–7594, 2019.

[16] T. Vigneysh and N. Kumarappan, “Autonomous operation and control of photovoltaic/solid oxide fuel cell/battery energy storage based microgrid using fuzzy logic controller,” *Int. J. Hydrogen Energy*, vol. 41, no. 3, pp. 1877–1891, 2016.

[17] W. Gil-González, F. Serra, J. Dominguez, J. Campillo, and O. Montoya, “Predictive power control for electric vehicle charging applications,” in *2020 IEEE ANDESCON*, 2020, pp. 1–6.

[18] I. Alhurayyis, A. Elkhateb, and D. J. Morrow, “Bidirectional DC-DC Resonant Converter Design for Electric Vehicle Charging Stations Integration to MVDC Grids,” in *2020 9th International Conference on Renewable Energy Research and*

Application (ICRERA), 2020, pp. 236–241.

[19] P. Sivaraman, T. Logeswaran, J. S. S. S. Raj, and S. Boopathimanikandan, "Design and Analysis of Sliding Mode Control for Battery Charging Applications," in *IOP Conference Series: Materials Science and Engineering*, 2020, vol. 995, no. 1, p. 12002.

[20] F. M. Shakeel and O. P. Malik, "Vehicle-To-Grid Technology in a Micro-grid Using DC Fast Charging Architecture," in *2019 IEEE Canadian Conference of Electrical and Computer Engineering (CCECE)*, 2019, pp. 1–4.

[21] R. Rajasekaran and P. U. Rani, "Bidirectional DC-DC converter for microgrid in energy management system," *Int. J. Electron.*, vol. 108, no. 2, pp. 322–343, 2021.

[22] A. M. Humada, M. Hojabri, S. Mekhilef, and H. M. Hamada, "Solar cell parameters extraction based on single and double-diode models: A review," *Renew. Sustain. Energy Rev.*, vol. 56, pp. 494–509, 2016.

[23] J. P. Torreglosa, P. García-Triviño, L. M. Fernández-Ramirez, and F. Jurado, "Decentralized energy management strategy based on predictive controllers for a medium voltage direct current photovoltaic electric vehicle charging station," *Energy Convers. Manag.*, vol. 108, pp. 1–13, 2016.

[24] A. Khamis, M. R. Ab Ghani, G. C. Kim, M. S. M. Aras, M. A. Bin Zabide, and T. Sutikno, "Control Strategy for Distributed Integration of Photovoltaic and Battery Energy Storage System in Micro-grids," *Telkomnika*, vol. 16, no. 5, pp. 2415–2427, 2018.

[25] M. O. Badawy, "Grid Tied PV/Battery System Architecture and Power Management for Fast Electric Vehicles Charging." University of Akron, 2016.

[26] F. Mwasilu, J. J. Justo, E.-K. Kim, T. D. Do, and J.-W. Jung, "Electric vehicles and smart grid interaction: A review on vehicle to grid and renewable energy sources integration," *Renew. Sustain. energy Rev.*, vol. 34, pp. 501–516, 2014.

[27] G. Angelov, M. Andreev, and N. Hinov, "Modelling of electric vehicle charging station for DC fast charging," in *2018 41st International Spring Seminar on Electronics Technology (ISSE)*, 2018, pp. 1–5.

[28] J. A. Mane and A. M. Jain, "Design, modelling and control of bidirectional DC-DC converter (for EV)," in *2015 International Conference on Emerging Research in Electronics, Computer Science and Technology (ICERECT)*, 2015, pp. 294–297.

[29] K. Tytelmaier, O. Husev, O. Veligorskyi, and R. Yershov, "A Review of Non-Isolated Bidirectional DC-DC Converters for Energy Storage Systems," pp. 22–28, 2016.

[30] A. Arancibia and K. Strunz, "Modeling of an electric vehicle charging station for fast DC charging," in *2012 IEEE International Electric Vehicle Conference*, 2012, pp. 1–6.

[31] M.-Y. Park, M.-H. Chi, J.-H. Park, H.-G. Kim, T.-W. Chun, and E.-C. Nho, "LCL-filter design for grid-connected PCS using total harmonic distortion and ripple attenuation factor," in *The 2010 International Power Electronics Conference-ECCE ASIA-*, 2010, pp. 1688–1694.

[32] M. K. Siddiqui, M. A. Mallick, and A. Iqbal, "Performance analysis of closed loop control of diesel generator power supply for base transceiver (BTS) load," 2019.

[33] Y. Shan, J. Hu, K. W. Chan, Q. Fu, and J. M. Guerrero, "Model predictive control of bidirectional DC–DC converters and AC/DC interlinking converters—A new control method for PV-wind-battery microgrids," *IEEE Trans. Sustain. Energy*, vol. 10, no. 4, pp. 1823–1833, 2018.

[34] V. Castiglia, P. Livreri, R. Miceli, F. R. Galluzzo, G. Santelia, and G. Schettino, "Design and simulation of a fast DC recharging station for EV," in *2017 IEEE 6th International Conference on Renewable Energy Research and Applications (ICRERA)*, 2017, pp. 1198–1203.

[35] D. Arcos-Aviles *et al.*, “An energy management system design using fuzzy logic control: Smoothing the grid power profile of a residential electro-thermal microgrid,” *IEEE Access*, vol. 9, pp. 25172–25188, 2021.

[36] K. Li, Y. Yang, S.-C. Tan, and R. S.-Y. Hui, “Sliding-mode-based direct power control of dual-active-bridge DC-DC converters,” in *2019 IEEE Applied Power Electronics Conference and Exposition (APEC)*, 2019, pp. 188–192.

[37] S.-C. Tan, Y.-M. Lai, K. T. Chi, L. Martínez-Salamero, and C.-K. Wu, “A fast-response sliding-mode controller for boost-type converters with a wide range of operating conditions,” *IEEE Trans. Ind. Electron.*, vol. 54, no. 6, pp. 3276–3286, 2007.

[38] N. Koduri, S. Kumar, and R. Y. Udaykumar, “On-board Vehicle-to-Grid (V2G) integrator for power transaction in smart grid environment,” in *2014 IEEE International Conference on Computational Intelligence and Computing Research*, 2014, pp. 1–4.

[39] S. A. Zulkifli, A. M. Mohammed, and F. Y. Tascikaraoglu, “Study Case: D-STATCOM in Low-Cost Hardware in the Loop for Voltage Sag Mitigation,” in *2021 IEEE International Conference in Power Engineering Application (ICPEA)*, 2021, pp. 30–34.

[40] A. Megha, N. Mahendran, and R. Elizabeth, “Analysis of Harmonic Contamination in Electrical Grid due to Electric Vehicle Charging,” in *2020 Third International Conference on Smart Systems and Inventive Technology (ICSSIT)*, 2020, pp. 608–614.

[41] G.-Y. Choe, J.-S. Kim, B.-K. Lee, C.-Y. Won, and T.-W. Lee, “A Bi-directional battery charger for electric vehicles using photovoltaic PCS systems,” in *2010 IEEE Vehicle Power and Propulsion Conference*, 2010, pp. 1–6.